

Extraordinary Magnetic Response of an Anisotropic 2D Antiferromagnet via Site Dilution

Junyi Yang, Hidemaro Suwa,* Derek Meyers, Han Zhang, Lukas Horak, Zhan Zhang, Evguenia Karapetrova, Jong-Woo Kim, Philip J. Ryan, Mark P. M. Dean, Lin Hao,* and Jian Liu*

Cite This: <https://doi.org/10.1021/acs.nanolett.3c02470>

Read Online

ACCESS |

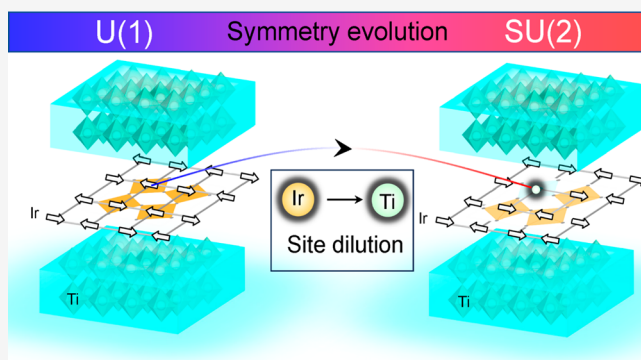
Metrics & More

Article Recommendations

Supporting Information

ABSTRACT: A prominent characteristic of 2D magnetic systems is the enhanced spin fluctuations, which reduce the ordering temperature. We report that a magnetic field of only 1000th of the Heisenberg superexchange interaction can induce a crossover, which for practical purposes is the effective ordering transition, at temperatures about 6 times the Néel transition in a site-diluted two-dimensional anisotropic quantum antiferromagnet. Such a strong magnetic response is enabled because the system directly enters the antiferromagnetically ordered state from the isotropic disordered state, skipping the intermediate anisotropic stage. The underlying mechanism is achieved on a pseudospin-half square lattice realized in the $[(\text{SrIrO}_3)_1/(\text{SrTiO}_3)_2]$ superlattice thin film that is designed to linearly couple the staggered magnetization to external magnetic fields by virtue of the rotational symmetry-preserving Dzyaloshinskii–Moriya interaction. Our model analysis shows that the skipping of the anisotropic regime despite finite anisotropy is due to the enhanced isotropic fluctuations under moderate dilution.

KEYWORDS: 2D antiferromagnet, heterostructure thin film, extraordinary magnetic response, magnetic dilution



Our model analysis shows that the skipping of the anisotropic regime despite finite anisotropy is due to the enhanced isotropic fluctuations under moderate dilution.

Past decades have seen tremendous breakthroughs in pursuing ultrafast and securer electronics based on antiferromagnetic (AFM) materials. However, finding of an efficient way to tune the AFM order parameter remains one of the biggest challenges.^{1,2} Stabilizing or controlling an AFM order requires the ability of suppressing or tuning the underlying spin fluctuations.³ For instance, in a two-dimensional (2D) isotropic antiferromagnet, the strong long-wavelength fluctuation prevents long-range order at finite temperatures. Suppression of such fluctuations can, in principle, be achieved by a staggered magnetic field. The impact of such a staggered field over the stability of the long-range order can be quantified by a characteristic length scale λ_{ext} , which represents the minimal length scale that the correlation length ξ must reach to exploit the Zeeman energy. On the other hand, the foremost character of spin fluctuations is their symmetry associated with magnetic anisotropy.^{4,5} Specifically, as temperature decreases, the rapidly increasing ξ could reach the length scale λ_{ani} characteristic of the magnetic anisotropy energy first ($\lambda_{\text{ext}} > \lambda_{\text{ani}}$) (Figure 1A). At that point, the magnetic anisotropy becomes the prime perturbation of the magnetic system. As a result, easy-axis or easy-plane anisotropy necessarily leads to slower divergences of ξ as the system cools below a certain temperature in contrast to the strong exponential divergence in the isotropic limit ($\lambda_{\text{ani}} = \infty$)

(Figure 1A).⁵ Since the finite anisotropy in real materials usually suffices to outcompete the Zeeman field ($\lambda_{\text{ext}} > \lambda_{\text{ani}}$),⁶ a strong field-induced response is difficult to realize, not to mention that it is nontrivial to realize a staggered magnetic field.

In this work, we present a proof-of-concept study showing that the AFM tunability can be systematically and significantly enhanced by exploiting magnetic dilution in the 2D antiferromagnets, giving rise to an over 600% increase of the AFM onset temperature with a magnetic field less than 0.5 T. Our pristine 2D antiferromagnet is realized on a pseudospin one-half square lattice embedded in a $[(\text{SrIrO}_3)_1/(\text{SrTiO}_3)_2]$ superlattice (SL), i.e., an ultrathin film of the $\text{Sr}_3\text{IrTi}_2\text{O}_9$ artificial crystal, where the neighboring IrO_2 planes are well separated by a nonmagnetic spacer.⁷ The strong spin–orbit coupling of Ir^{4+} ions stabilizes onsite $J_{\text{eff}} = 1/2$ moments^{8–10} that couple antiferromagnetically via Heisenberg superexchange interactions J .^{7,11} A key character of such a $J_{\text{eff}} =$

Received: July 5, 2023

Revised: November 9, 2023

Accepted: November 9, 2023

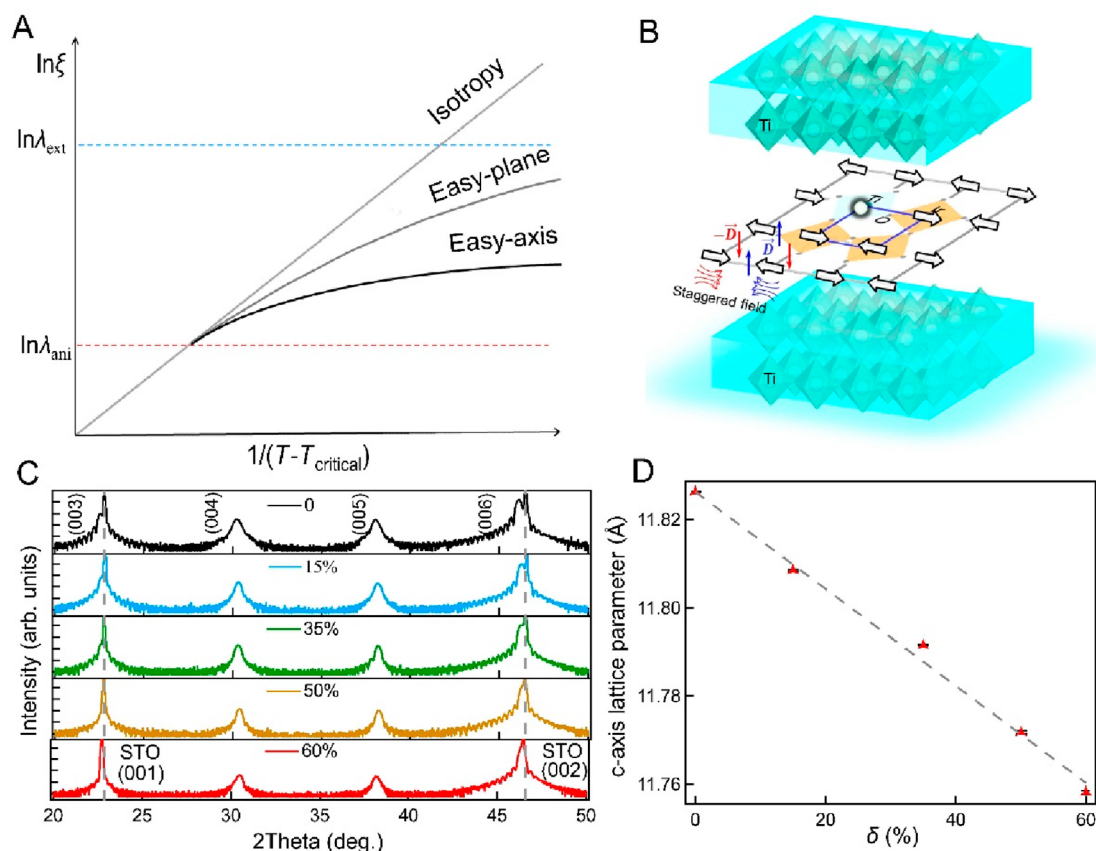


Figure 1. Crystal structure of diluted 2D antiferromagnets. (A) Temperature-dependences of ξ for different 2D magnetic systems. (B) Schematic diagram of the $[(\text{SrIr}_{1-\delta}\text{Ti}_\delta\text{O}_3)/(\text{SrTiO}_3)_2]$ SL. (C) Theta-2Theta X-ray diffraction (XRD) patterns of the SLs. The SL Bragg peaks are defined in the $a \times a \times 3c$ superstructure cell, where a and c are the pseudocubic in-plane and out-of-plane lattice parameters, respectively. (D) c -Axis lattice parameter, determined from synchrotron XRD around the (0 0 18) Bragg reflections [Supplementary Figure S1], as a function of δ . The error bars are deduced from experimental statistics. Dashed lines denote the expected lattice parameters. All the SLs share the same in-plane lattice parameters with the SrTiO_3 substrate, as confirmed from reciprocal space mapping measurements [Supplementary Figure S2].

$1/2$ square lattice is that the large local Dzyaloshinskii–Moriya interaction D ,^{12,13} arising from the staggered IrO_6 octahedral rotation around the c -axis, tends to cancel over the lattice as a whole such that the pseudospins are overall almost completely isotropic—a phenomenon called hidden $\text{SU}(2)$ symmetry (Figure 1B).^{14–17} This further allows an in-plane uniform magnetic field h to act as an effective staggered field $h \cdot \sin \varphi$, with $\tan(2\varphi) = D/J$.^{11,18} However, the high-order superexchange paths due to Hund's coupling induce a small easy-plane anisotropy and practically lower the spin symmetry from $\text{SU}(2)$ to $\text{U}(1)$,¹⁶ leading to an AFM transition at ~ 40 K by virtue of the large J and the tiny yet finite interplane coupling.¹¹ The SL is nevertheless a weakly anisotropic Heisenberg antiferromagnet in the proximity of the 2D limit.

To introduce magnetic dilution, we partially substituted Ir^{4+} ions with isovalent nonmagnetic Ti^{4+} ions by a nominal dilution percentage δ during the atomic layer-by-layer deposition (Figure 1B) [see Supplementary for details about materials synthesis]. Figure 1C lists the XRD patterns of the SL series, where the same set of Bragg reflections can be seen, indicating that the SLs are single-phase and epitaxially oriented along the [001] direction. The c -axis lattice parameter c_{SL} decreases monotonically with δ , consistent with the expected dependence on the volume fraction change,¹⁹ i.e., $c_{\text{SL}} = 3\delta \times c_{\text{STO}} + (1 - \delta) \times c_{\text{pristine}}$ where c_{STO} and c_{pristine} are the c -axis lattice parameters of SrTiO_3 and the $\delta = 0$ SL, respectively

(Figure 1D). By comparing the experimental c_{SL} and the expected c_{SL} , we calibrated δ , which turned out to be very close to the nominal values with a very small error bar [Supplementary Table S1]. For simplicity, we use the nominal values of δ in the subsequent discussion. Note that magnetic dilution leaves the global crystal symmetry invariant [Supplementary Figure S3].

To further probe the AFM order in such ultrathin samples (~ 36 nm), we exploited a magnetic resonant X-ray scattering technique. As shown in Figure 2A, the (0.5 0.5 5) magnetic peak was observed on each SL at the base temperature, demonstrating that the AFM checkerboard type ground state⁷ is preserved even under a substantial magnetic dilution. The peak intensity, which is proportional to the order parameter squared, decreases monotonically with δ , which we assign to both enhanced spin fluctuations and reduced Ir^{4+} content due to dilution. Figure 2C shows thermal evolutions of the magnetic order parameter (the square root of the peak intensity). One can see that increasing δ significantly suppresses the AFM transition, confirming the escalated AFM fluctuations. The Néel temperature T_{N} is assigned as the onset temperature of the Bragg peak and plotted against δ in Figure 2B. Interestingly, extrapolation of the δ dependence of T_{N} estimates that the AFM order would collapse at $\delta \sim 60\%$, which is markedly close to the theoretical percolation threshold $p_c \approx 0.593$ of a site-diluted square lattice with

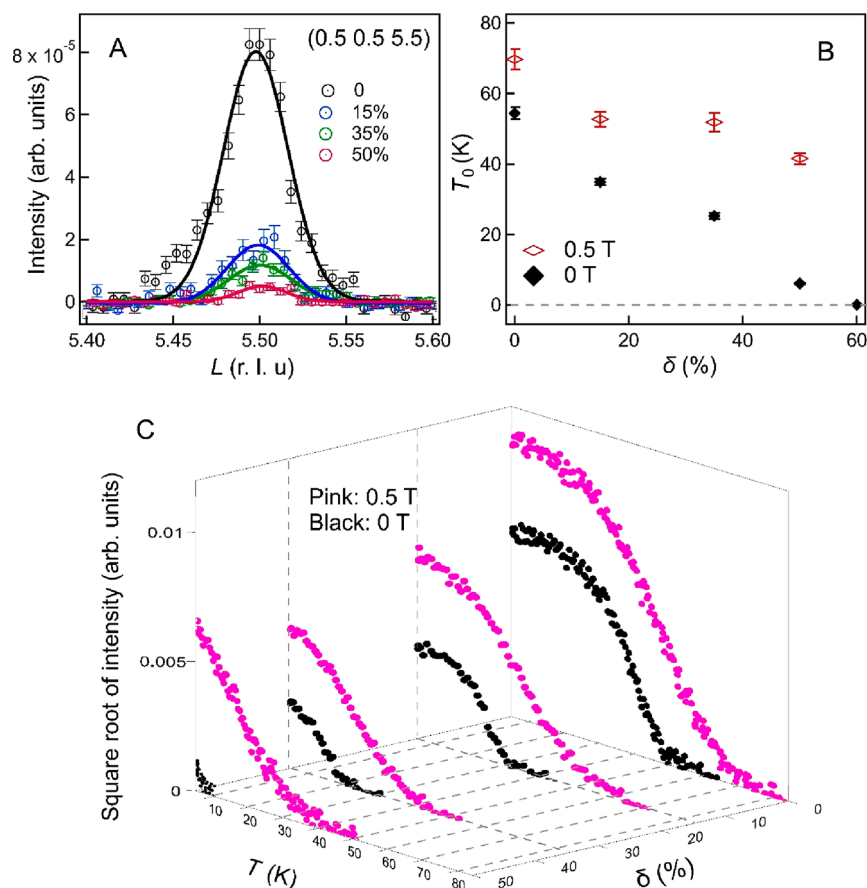


Figure 2. Magnetic scattering measurements on the diluted SLs. (A) Base-temperature (~ 5 K) L -scans across the (0.5 0.5 5) magnetic reflection under 0 T of the SLs. (B) T_N and T_0 ($B = 0.5$ T) as a function of δ . (C) Temperature-dependent square root of the magnetic peak intensity, which characterizes the AFM order parameter, under 0 (black) and 0.5 T (pink).

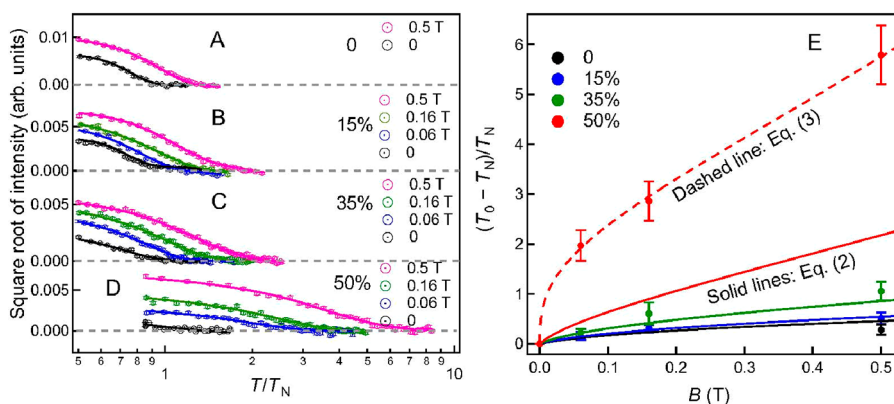


Figure 3. AFM response to magnetic field and theoretical analysis. Square root of peak intensity versus T/T_N for $\delta = 0$ (A), 15% (B), 35% (C), and 50% (D), under various magnetic fields. Error bars represent the statistic error. (E) $(T_0 - T_N)/T_N$ versus magnetic field, where $T_0(B = 0) = T_N$. Solid curves are theoretical analysis for $\delta = 0$ (black), 15% (blue), 35% (green), and 50% (red) using eq 2. For $\delta = 50\%$, simulation using eq 3 is also shown (dashed).

both nearest-neighboring and next nearest-neighboring interactions.²⁰ As a comparison, the AFM order of a diluted square-lattice cuprate disappears around the theoretical value $p_c \approx 0.407$ with the nearest-neighboring interaction only.²¹ The relatively larger next-nearest neighboring interaction between Ir sites over the cuprates has been confirmed on various iridates.^{22–24}

The effect of magnetic dilution is more pronounced in the presence of an in-plane magnetic field. In consistency with T_N

defined at zero field, we define the onset temperature under nonzero magnetic field as the crossover temperature T_0 . As shown in Figure 2C, T_0 is increased by $\sim 30\%$ in the pristine SL when applying a field of 0.5 T because of the effective staggered field effect in suppressing the 2D fluctuations of the AFM order.¹¹ When the magnetic dilution is introduced, this enhancement is doubled to $\sim 60\%$ at $\delta = 15\%$. It continues to increase at $\delta = 35\%$ and reaches $\sim 600\%$ at $\delta = 50\%$, which manifests as an extremely efficient tuning of the AFM order by

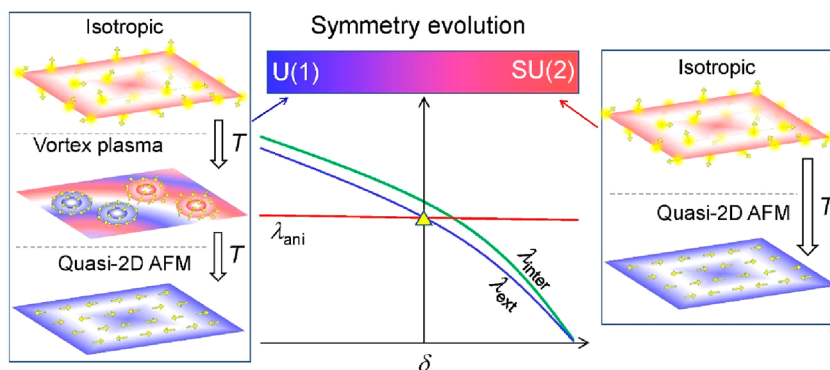


Figure 4. Schematic diagram of the site dilution induced spin symmetry evolution and temperature-dependent phase change. For δ smaller than the crossing point marked by a triangle, where λ_{ani} is comparable to λ_{ext} , the system transitions from the high-temperature isotropic state to the quasi-2D AFM ground state via an intermediate vortex plasma phase accounting for the U(1) spin symmetry. If δ is larger than the marked value, the isotropic state directly crosses over into the ground state unveiling an effective SU(2) spin symmetry.

suppressing the enhanced fluctuations. When comparing the energy scale, the enhanced thermal stability of the AFM order (~ 10 K) is at least 1 order of magnitude larger than the Zeeman energy of 0.5 T, highlighting the fact that the AFM order responds to the magnetic field in the nontrivial manner. Moreover, since the AFM order is stabilized by the staggered field component in the plane produced by the staggered octahedral rotation about the z -axis, the large magnetic response achieved under a small in-plane magnetic field also excludes the possible effect of the field enforced XY-fluctuation.^{25–28}

To quantify this effect, we measured the temperature dependence by systematically increasing the field from 0, to 0.06, to 0.16, and finally to 0.5 T. Figure 3A–D compares the thermal evolutions on the normalized temperature scale T/T_N . One can clearly see that the T_0/T_N is systematically increased with the applied in-plane field at all the δ values, and a larger δ is beneficial for the T_0 enhancement under the same magnetic field. It is noteworthy that the magnetic response is especially significant at small fields and is drastically increased with increasing δ . For example, 0.06 T increases T_0 of the $\delta = 50\%$ SL by ~ 12 K ($T_0/T_N \approx 3$), which is 200 times larger than the applied Zeeman energy. Figure 3E summarizes the field dependence of the normalized increase $(T_0 - T_N)/T_N$ with different δ values ($T_0 = T_N$ at zero field). This quantitative comparison not only further confirms the dilution-enhanced magnetic response but also shows that the enhancement is particularly large at $\delta = 50\%$ with an extremely sharp increase of $(T_0 - T_N)/T_N$ at small fields (see Supplementary Figure S7 for an alternative way of defining T_N and T_0 that leads to the same conclusion). This exceptional behavior points to a possible change of the fluctuation nature under a moderate dilution.

We conduct a theoretical analysis of T_0 under dilution, which indeed confirms a change in the fluctuation from the anisotropic BKT regime to the isotropic regime. Specifically, to obtain an analytic expression of T_0 , one must consider and compare the characteristic length scales of three perturbative interactions, which include the weak easy-plane anisotropy $\Gamma_1 \approx 10^{-4}J$, the interplane coupling $|J_\perp| \approx 10^{-5}J$, and the Zeeman energy $h \cdot \sin \varphi$ ¹¹ [Supplementary]. First, in a 2D system with easy-plane anisotropy, the Berezinskii–Kosterlitz–Thouless (BKT) transition occurs at T_{BKT} , above which the vortex is antibonding and below which the vortex pair forms a bonding state.²⁹ The vortex is a classical solution in the continuum limit

of the 2D easy-plane model. Here the vortex size is the well-defined length scale of anisotropy: $\lambda_{\text{ani}} \sim 1/\sqrt{\Gamma_1}$. Second, from the scaling argument,²⁹ the crossover from the 2D system to the effective 3D system occurs when the condition $2(1 - \delta)^2 |J_\perp| S^2 \xi^2 \sim 2\pi\rho_s$ is satisfied, where ρ_s is the spin stiffness at $T = 0$, defining the length scale of interplane coupling $\lambda_{\text{inter}} \sim \sqrt{\pi\rho_s/(1 - \delta)^2 |J_\perp| S^2}$. Third, the effective staggered field introduces another length scale in a way similar to the interplane coupling: $\lambda_{\text{ext}} \sim \sqrt{2\pi\rho_s/(1 - \delta) |h \sin \varphi| S}$. Note that λ_{inter} and λ_{ext} can be defined regardless of the spin anisotropy strength. Thanks to the 2D nature of the SL, $|J_\perp| < |h \sin \varphi|$ is achieved even at 0.06 T, leading to $\lambda_{\text{ext}} < \lambda_{\text{inter}}$ ^{7,11}

In the pristine system ($\delta = 0$), we find $\lambda_{\text{ani}} < \lambda_{\text{ext}} < \lambda_{\text{inter}}$, where $\lambda_{\text{ani}} \sim 100$, $\lambda_{\text{ext}} \sim 300$ for 0.06 T, and $\lambda_{\text{inter}} \sim 400$ in units of the in-plane lattice parameter. Thus, as ξ increases with decreasing temperature, the high-temperature disordered and isotropic state first crosses over to the 2D easy-plane state, where independent vortices are created (see the left panel of Figure 4 for a schematic illustration), when $\xi \sim \lambda_{\text{ani}}$. The crossover to the 3D ordered state eventually takes place at a lower temperature such that the vortex-pair creation energy becomes comparable to the energy cost induced by J_\perp and h .²⁹ This condition when adapted for the diluted system is expressed by

$$2(1 - \delta)^2 |J_\perp| S^2 + (1 - \delta) |h \sin \varphi| S \xi^2 \sim 2\rho_s \ln \xi \quad (1)$$

In the 2D system with the preformed vortex, the correlation length diverges in the form $\xi \sim e^{b/\sqrt{t}}$, where b is a constant depending on Γ_1 but not on δ , and $t = \frac{T - T_{\text{BKT}}}{T_{\text{BKT}}}$.²⁹ Using $\rho_s(T = 0) \propto \rho_s(T_{\text{BKT}})$ and the Nelson–Kosterlitz relation $\rho_s(T_{\text{BKT}}) = \frac{2}{\pi} T_{\text{BKT}}$, we formulate the crossover temperature of the U(1) model

$$T_0 = T_{\text{BKT}} + \frac{4b^2 T_{\text{BKT}}}{\left[\ln \left(\frac{c T_{\text{BKT}}}{2(1 - \delta)^2 |J_\perp| S^2 + (1 - \delta) |h \sin \varphi| S} \right) \right]^2} \quad (2)$$

where c is a constant in the prefactor of the scaling. From our quantum Monte Carlo simulations [Supplementary], we obtained $\frac{T_{\text{BKT}}}{J} \approx 0.213, 0.122, \text{ and } 0.0339$ for $\delta = 0, 15\%, \text{ and } 35\%$, respectively, and $b \approx 3.4$ commonly.

$\bar{J} = \sqrt{J^2 + D^2} \approx 600$ K where $\frac{D}{J} = 0.27$. We estimate $|J_{\perp}| \approx 0.006$ K and $c \approx 0.2$, which are consistent with the previous estimates.¹¹ Eq 2 reproduces well the increase of $(T_0 - T_N)/T_N$ for all SLs with $\delta \lesssim 35\%$ as seen as the solid lines in Figure 3e. However, a large deviation is clearly seen for $\delta = 50\%$: the theoretical curve of eq 2 is significantly lower than the experimental result, indicating that the U(1) model fails in this SL. We found this conclusion very robust since our extended theoretical calculations show that this deviation does not result from error in δ , and simply adjusting δ in eq 2 does not reproduce the observed response of the $\delta = 50\%$ SL [Supplementary Figure S6]. We argue here that this is because the moderate magnetic dilution changes the picture drastically. In the diluted system, T_N and ρ_s significantly decrease. Accordingly, λ_{inter} and λ_{ext} are greatly reduced. On the other hand, as we numerically confirmed [Supplementary Figure S5], λ_{ani} is almost independent of δ , because λ_{ani} is well-defined in the vortex solution of the continuum limit, where the reduction of the effective coordination number is irrelevant. This is consistent with previous studies on diluted quasi-2D antiferromagnets, which reveal that the anisotropy-related critical behavior around magnetic transition is not fundamentally changed by magnetic dilution.^{30,31} Therefore, one would acquire the situation of $\lambda_{\text{ext}} < \lambda_{\text{inter}}, \lambda_{\text{ani}}$ at a sufficiently large δ even for a tiny field. The vortex-bonding picture is invalid in this regime, because independent vortices are never created. Instead, the crossover emerges directly from the 2D isotropic state to the AFM ordered state (as shown in the right panel of Figure 4) when the scaling relation $(1 - \delta)h \sin \phi S \xi^2 \sim 2\pi\rho_s$ is satisfied. $\xi \sim e^{2\pi\rho_s/T}$ follows the exponential divergence of the 2D Heisenberg model in the “renormalized classical” regime.^{32,33} As a result, compared to eq 1, the vortex-pair creation energy is replaced with the skyrmion (Meron-pair) creation energy,^{34,35} which is independent of ξ . T_0 in this regime is given by

$$T_0 = \frac{4\pi\rho_s}{\ln\left(\frac{a\rho_s}{d + (1 - \delta)h \sin \phi S}\right)} \quad (3)$$

where a and d are constants that stem from the prefactor of the scaling relation and from the effect of other perturbations, respectively (Supplementary). For $\delta = 50\%$, we estimate $a \approx 0.1$ and $d \approx 10^{-6}$ K. The analytical forms eq 2 and eq 3 highlight the significant difference between the two regimes. Explicitly speaking, the asymptotic scaling of T_0 in the vortex-bonding regime is given by $\frac{T_0 - T_N}{T_N} \propto \frac{1}{\left(\ln \frac{\rho_s}{h}\right)^2}$, while the scaling relation is replaced by $\frac{T_0 - T_N}{T_N} \propto \frac{1}{\ln \frac{\rho_s}{h}}$ in the isotropic regime.

Since $\frac{1}{\ln \frac{\rho_s}{h}}$ is always smaller than 1 for all dilution levels, the field response in the isotropic regime is significantly enhanced under the same magnetic fields.

This regime governed by 2D isotropic fluctuations is expected to be valid for the case of $\delta = 50\%$. Using the quantum Monte Carlo method,^{36,37} we obtain $\rho_s(\delta = 50\%) \approx 0.02\rho_s(\delta = 0)$ at $T = 0$, giving rise to $\lambda_{\text{ani}} \sim \lambda_{\text{inter}} \sim 100$ and $\lambda_{\text{ext}} \sim 70$ for 0.06 T. This explicitly demonstrates that we indeed achieved $\lambda_{\text{ext}} < \lambda_{\text{inter}}, \lambda_{\text{ani}}$. This switching also takes advantage of antiferromagnets, which in general have much reduced spin stiffness compared to ferromagnetic materials. As shown in

Figure 3e, the dashed line from eq 3 not only accounts for the rapid increase of $(T_0 - T_N)/T_N$ at small fields for the $\delta = 50\%$ SL but also reasonably reproduces the whole field dependence. As compared to the U(1) model of eq 2, the supremacy of the SU(2) model on explaining the experimental observation thus confirms the emergence of the isotropic fluctuations in the moderately diluted SL. Because $\delta = 50\%$ is approximately 10% less than the percolation threshold, this SL is expected to be outside of the quantum critical regime.²¹ We emphasize that the enormous SU(2) symmetric fluctuations emerging from the highly correlated low-temperature state are realized in the 2D renormalized classical regime and thus essentially differ from the ordinary fluctuations in uncorrelated high-temperature states. Furthermore, while spin fluctuations in diluted anisotropic 2D antiferromagnets have been extensively studied,^{19,21,30,31} the ability to switch length scales of anisotropy and external field has not been achieved, largely due to the lack of an effective staggered field effect. It can be realized in our SLs because all the necessary ingredients, including the dimensionality, the dilution, and the hidden symmetry, are implemented through top-down design and bottom-up synthesis, pointing to a new approach to studying spin fluctuations in quasi-2D magnets that are unobtainable in bulk synthesis.

In summary, we demonstrate a general and powerful idea of switching the order of the characteristic length scales in 2D magnets through magnetic dilution on atomic-scale. The symmetry of spin fluctuations that we can utilize by applying magnetic field changes from U(1) to SU(2) in an anisotropic 2D pseudospin-half quantum antiferromagnet under moderate dilution. The zero-energy long-wavelength spin excitation is thus extremely sensitive to small stimuli, demonstrated here by virtue of the effective staggered magnetic field effect due to strong spin-orbit coupling. An extraordinary field-induced AFM ordering temperature increase in a moderately diluted SL was observed. Our idea of the length-scale switch can be applied to easy-axis systems as well. Since dilution effects due to dopants and disorder are common in many quantum materials, these results are of intrinsic interest for both fundamental understanding and operational control of low-dimensional magnets, especially near quantum phase transitions.

■ ASSOCIATED CONTENT

SI Supporting Information

The Supporting Information is available free of charge at <https://pubs.acs.org/doi/10.1021/acs.nanolett.3c02470>.

Synthesis details, calculations, and additional figures (PDF)

■ AUTHOR INFORMATION

Corresponding Authors

Jian Liu – Department of Physics and Astronomy, University of Tennessee, Knoxville, Tennessee 37996, United States; Email: jianliu@utk.edu

Hidemaro Suwa – Department of Physics, University of Tokyo, Tokyo 113-0033, Japan; orcid.org/0000-0002-6026-2630; Email: suwaro@phys.s.u-tokyo.ac.jp

Lin Hao – Anhui Key Laboratory of Condensed Matter Physics at Extreme Conditions, High Magnetic Field Laboratory, HFIPS, Chinese Academy of Sciences, Hefei, Anhui 230031, China; Email: haolin@hmfl.ac.cn

Authors

Junyi Yang – Department of Physics and Astronomy, University of Tennessee, Knoxville, Tennessee 37996, United States; Present Address: Material Science Division, Argonne National Laboratory, Lemont, Illinois 60439, USA; orcid.org/0000-0001-9074-6030

Derek Meyers – Department of Condensed Matter Physics and Materials Science, Brookhaven National Laboratory, Upton, New York 11973, United States; Department of Physics, Oklahoma State University, Stillwater, Oklahoma 74078, United States

Han Zhang – Department of Physics and Astronomy, University of Tennessee, Knoxville, Tennessee 37996, United States

Lukas Horak – Department of Condensed Matter Physics, Charles University, 12116 Prague, Czech Republic

Zhan Zhang – Advanced Photon Source, Argonne National Laboratory, Lemont, Illinois 60439, United States

Evguenia Karapetrova – Advanced Photon Source, Argonne National Laboratory, Lemont, Illinois 60439, United States

Jong-Woo Kim – Advanced Photon Source, Argonne National Laboratory, Lemont, Illinois 60439, United States

Philip J. Ryan – Advanced Photon Source, Argonne National Laboratory, Lemont, Illinois 60439, United States; School of Physical Sciences, Dublin City University, Dublin 9, Ireland

Mark P. M. Dean – Department of Condensed Matter Physics and Materials Science, Brookhaven National Laboratory, Upton, New York 11973, United States

Complete contact information is available at:

<https://pubs.acs.org/10.1021/acs.nanolett.3c02470>

Funding

J.L. acknowledges support from the National Science Foundation under Grant No. DMR-1848269. M.P.M.D. is supported by the U.S. Department of Energy, Office of Basic Energy Sciences, Early Career Award Program under Award No. 1047478. L. Horak acknowledges the support by the ERDF (project CZ.02.1.01/0.0/0.0/15_003/0000485) and the Grant Agency of the Czech Republic grant (14-37427 G). Use of the Advanced Photon Source, an Office of Science User Facility operated for the US DOE, OS by Argonne National Laboratory, was supported by the U.S. DOE under contract no. DE-AC02-06CH11357. Work at Brookhaven is supported by the Office of Basic Energy Sciences, Materials Sciences and Engineering Division, U.S. Department of Energy (DOE) under Contract No. DE-SC0012704. H.S. acknowledges Inamori Research Grants from the Inamori Foundation and support from JSPS KAKENHI Grant Nos. JP19K14650 and JP22K03508. L. Hao acknowledges support from the international partnership program of the Chinese Academy of Sciences (145GJHZ2022044MI), the Collaborative Innovation Program of Hefei Science Center, Chinese Academy of Sciences (2022HSC-CIP005), the HFIPS Director's Fund (2023YZGH01), the Basic Research Program of the Chinese Academy of Sciences Based on Major Scientific Infrastructures (grant No. JZHKYPT-2021-08), and the National Natural Science Foundation of China (12104460). Simulations were performed using computational resources of the Supercomputer Center at the Institute for Solid State Physics, the University of Tokyo. A portion of this work was performed on the Steady High Magnetic Field Facilities, CAS, and supported by the High Magnetic Field Laboratory of Anhui Province.

Notes

The authors declare no competing financial interest.

ACKNOWLEDGMENTS

The authors acknowledge experimental assistance from H. D. Zhou and M. Koehler. L. Hao appreciates helpful discussions with H. Zhu.

REFERENCES

- (1) Song, C.; You, Y.; Chen, X.; Zhou, X.; Wang, Y.; Pan, F. How to manipulate magnetic states of antiferromagnets. *Nanotechnology* **2018**, *29* (11), 112001.
- (2) Jungfleisch, M. B.; Zhang, W.; Hoffmann, A. Perspectives of antiferromagnetic spintronics. *Phys. Lett. A* **2018**, *382* (13), 865–871.
- (3) Blundell, S. *Magnetism in condensed matter*; OUP Oxford: 2001.
- (4) Vasiliev, A.; Volkova, O.; Zvereva, E.; Markina, M. Milestones of low-D quantum magnetism. *npj Quantum Mater.* **2018**, *3* (1), 18.
- (5) Gibertini, M.; Koperski, M.; Morpurgo, A. F.; Novoselov, K. S. Magnetic 2D materials and heterostructures. *Nat. Nanotechnol.* **2019**, *14* (5), 408–419.
- (6) Varma, C. M. Quantum-critical fluctuations in 2D metals: strange metals and superconductivity in antiferromagnets and in cuprates. *Rep. Prog. Phys.* **2016**, *79* (8), 082501.
- (7) Hao, L.; Meyers, D.; Frederick, C.; Fabbris, G.; Yang, J.; Traynor, N.; Horak, L.; Kriegner, D.; Choi, Y.; Kim, J.-W.; Haskel, D.; Ryan, P. J.; Dean, M. P. M.; Liu, J. Two-Dimensional Jeff = 1/2 Antiferromagnetic Insulator Unraveled from Interlayer Exchange Coupling in Artificial Perovskite Iridate Superlattices. *Phys. Rev. Lett.* **2017**, *119* (2), 027204.
- (8) Kim, B. J.; Ohsumi, H.; Komesu, T.; Sakai, S.; Morita, T.; Takagi, H.; Arima, T. Phase-Sensitive Observation of a Spin-Orbital Mott State in Sr₂IrO₄. *Science* **2009**, *323* (5919), 1329–1332.
- (9) Rau, J. G.; Lee, E. K.-H.; Kee, H.-Y. Spin-Orbit Physics Giving Rise to Novel Phases in Correlated Systems: Iridates and Related Materials. *Annu. Rev. Condens. Matter Phys.* **2016**, *7* (1), 195–221.
- (10) Cao, G.; Schlottmann, P. The challenge of spin–orbit-tuned ground states in iridates: a key issues review. *Rep. Prog. Phys.* **2018**, *81* (4), 042502.
- (11) Hao, L.; Meyers, D.; Suwa, H.; Yang, J.; Frederick, C.; Dasa, T. R.; Fabbris, G.; Horak, L.; Kriegner, D.; Choi, Y.; Kim, J.-W.; Haskel, D.; Ryan, P. J.; Xu, H.; Batista, C. D.; Dean, M. P. M.; Liu, J. Giant magnetic response of a two-dimensional antiferromagnet. *Nat. Phys.* **2018**, *14*, 806–810.
- (12) Dzyaloshinsky, I. A thermodynamic theory of “weak” ferromagnetism of antiferromagnetics. *J. Phys. Chem. Solids* **1958**, *4* (4), 241–255.
- (13) Moriya, T. Anisotropic superexchange interaction and weak ferromagnetism. *Phys. Rev.* **1960**, *120*, 91–98.
- (14) Shekhtman, L.; Entin-Wohlman, O.; Aharony, A. Moriya’s anisotropic superexchange interaction, frustration, and Dzyaloshinsky’s weak ferromagnetism. *Phys. Rev. Lett.* **1992**, *69* (5), 836–839.
- (15) Wang, F.; Senthil, T. Twisted Hubbard Model for Sr₂IrO₄: Magnetism and Possible High Temperature Superconductivity. *Phys. Rev. Lett.* **2011**, *106* (13), 136402.
- (16) Jackeli, G.; Khaliullin, G. Mott Insulators in the Strong Spin-Orbit Coupling Limit: From Heisenberg to a Quantum Compass and Kitaev Models. *Phys. Rev. Lett.* **2009**, *102* (1), 017205.
- (17) Fujiyama, S.; Ohsumi, H.; Komesu, T.; Matsuno, J.; Kim, B. J.; Takata, M.; Arima, T.; Takagi, H. Two-Dimensional Heisenberg Behavior of Jeff = 1/2 Isospins in the Paramagnetic State of the Spin-Orbital Mott Insulator Sr₂IrO₄. *Phys. Rev. Lett.* **2012**, *108* (24), 247212.
- (18) Hao, L.; Wang, Z.; Yang, J.; Meyers, D.; Sanchez, J.; Fabbris, G.; Choi, Y.; Kim, J.-W.; Haskel, D.; Ryan, P. J.; Barros, K.; Chu, J.-H.; Dean, M. P. M.; Batista, C. D.; Liu, J. Anomalous magneto-resistance due to longitudinal spin fluctuations in a Jeff = 1/2 Mott semiconductor. *Nat. Commun.* **2019**, *10* (1), 5301.

- (19) Cowley, R. A.; Shirane, G.; Birgeneau, R. J.; Guggenheim, H. J. Spin fluctuations in random magnetic-nonmagnetic two-dimensional antiferromagnets. I. Dynamics. *Phys. Rev. B* **1977**, *15* (9), 4292–4302.
- (20) Feng, X.; Deng, Y.; Blöte, H. W. J. Percolation transitions in two dimensions. *Phys. Rev. E* **2008**, *78* (3), 031136.
- (21) Vajk, O. P.; Mang, P. K.; Greven, M.; Gehring, P. M.; Lynn, J. W. Quantum Impurities in the Two-Dimensional Spin One-half Heisenberg Antiferromagnet. *Science* **2002**, *295* (5560), 1691–1695.
- (22) Kim, J.; Casa, D.; Upton, M. H.; Gog, T.; Kim, Y.-J.; Mitchell, J. F.; van Veenendaal, M.; Daghofer, M.; van den Brink, J.; Khaliullin, G.; Kim, B. J. Magnetic Excitation Spectra of SrIrO₄ Probed by Resonant Inelastic X-Ray Scattering: Establishing Links to Cuprate Superconductors. *Phys. Rev. Lett.* **2012**, *108* (17), 177003.
- (23) Meyers, D.; Cao, Y.; Fabbri, G.; Robinson, N. J.; Hao, L.; Frederick, C.; Traynor, N.; Yang, J.; Lin, J.; Upton, M. H.; Casa, D.; Kim, J.-W.; Gog, T.; Karapetrova, E.; Choi, Y.; Haskel, D.; Ryan, P. J.; Horak, L.; Liu, X.; Liu, J.; Dean, M. P. M. Magnetism in iridate heterostructures leveraged by structural distortions. *Sci. Rep.* **2019**, *9* (1), 4263.
- (24) Coldea, R.; Hayden, S. M.; Aeppli, G.; Perring, T. G.; Frost, C. D.; Mason, T. E.; Cheong, S. W.; Fisk, Z. Spin Waves and Electronic Interactions in La₂CuO₄. *Phys. Rev. Lett.* **2001**, *86* (23), 5377–5380.
- (25) Cuccoli, A.; Roscilde, T.; Vaia, R.; Verrucchi, P. Field-induced XY behavior in the $S = 1/2$ antiferromagnet on the square lattice. *Phys. Rev. B* **2003**, *68* (6), 060402.
- (26) Xiao, F.; Woodward, F. M.; Landee, C. P.; Turnbull, M. M.; Mielke, C.; Harrison, N.; Lancaster, T.; Blundell, S. J.; Baker, P. J.; Babkevich, P.; Pratt, F. L. Two-dimensional XY behavior observed in quasi-two-dimensional quantum Heisenberg antiferromagnets. *Phys. Rev. B* **2009**, *79* (13), 134412.
- (27) Tsyrlin, N.; Xiao, F.; Schneidewind, A.; Link, P.; Rønnow, H. M.; Gavilano, J.; Landee, C. P.; Turnbull, M. M.; Kenzelmann, M. Two-dimensional square-lattice $S = 1/2$ antiferromagnet Cu(pz)₂(ClO₄)₂. *Phys. Rev. B* **2010**, *81* (13), 134409.
- (28) Cuccoli, A.; Roscilde, T.; Vaia, R.; Verrucchi, P. Detection of XY Behavior in Weakly Anisotropic Quantum Antiferromagnets on the Square Lattice. *Phys. Rev. Lett.* **2003**, *90* (16), 167205.
- (29) Hikami, S.; Tsuneto, T. Phase transition of quasi-two dimensional planar system. *Prog. Theor. Phys.* **1980**, *63* (2), 387–401.
- (30) Birgeneau, R. J.; Cowley, R. A.; Shirane, G.; Tarvin, J. A.; Guggenheim, H. J. Spin fluctuations in random magnetic-nonmagnetic two-dimensional antiferromagnets. II. Heisenberg percolation. *Phys. Rev. B* **1980**, *21* (1), 317–332.
- (31) Cowley, R. A.; Birgeneau, R. J.; Shirane, G.; Guggenheim, H. J.; Ikeda, H. Spin fluctuations in random magnetic-nonmagnetic two-dimensional antiferromagnets. III. An Ising system. *Phys. Rev. B* **1980**, *21* (9), 4038–4048.
- (32) Chakravarty, S.; Halperin, B. I.; Nelson, D. R. Two-dimensional quantum Heisenberg antiferromagnet at low temperatures. *Phys. Rev. B* **1989**, *39* (4), 2344–2371.
- (33) Chubukov, A. V.; Sachdev, S.; Ye, J. Theory of two-dimensional quantum Heisenberg antiferromagnets with a nearly critical ground state. *Phys. Rev. B* **1994**, *49* (17), 11919–11961.
- (34) Tang, J.; Wu, Y.; Wang, W.; Kong, L.; Lv, B.; Wei, W.; Zang, J.; Tian, M.; Du, H. Magnetic skyrmion bundles and their current-driven dynamics. *Nat. Nanotechnol.* **2021**, *16* (10), 1086–1091.
- (35) Wang, W.; Song, D.; Wei, W.; Nan, P.; Zhang, S.; Ge, B.; Tian, M.; Zang, J.; Du, H. Electrical manipulation of skyrmions in a chiral magnet. *Nat. Commun.* **2022**, *13* (1), 1593.
- (36) Todo, S.; Matsuo, H.; Shitara, H. Parallel loop cluster quantum Monte Carlo simulation of quantum magnets based on global union-find graph algorithm. *Comput. Phys. Commun.* **2019**, *239*, 84–93.
- (37) Bauer, B.; Carr, L. D.; Evertz, H. G.; Feiguin, A.; Freire, J.; Fuchs, S.; Gamper, L.; Gukelberger, J.; Gull, E.; Guertler, S.; Hehn, A.; Igarashi, R.; Isakov, S. V.; Koop, D.; Ma, P. N.; Mates, P.; Matsuo, H.; Parcollet, O.; Pawłowski, G.; Picon, J. D.; Pollet, L.; Santos, E.; Scarola, V. W.; Schollwöck, U.; Silva, C.; Surer, B.; Todo, S.; Trebst, S.; Troyer, M.; Wall, M. L.; Werner, P.; Wessel, S. The ALPS project release 2.0: open source software for strongly correlated systems. *J. Stat. Mech.: Theor. Exp.* **2011**, *2011* (05), P05001.